Dalton Transactions

RSC Publishing

PAPER

View Article Online
View Journal | View Issue

Cite this: *Dalton Trans.*, 2013, **42**, 5932

Zinc(II) complexes containing bis-benzimidazole derivatives as a new class of apoptosis inducers that trigger DNA damage-mediated p53 phosphorylation in cancer cells†

Shenggui Liu,‡[a,b] Wenqiang Cao,‡[a] Lianling Yu,[a] Wenjie Zheng,*[a] Linlin Li,[a] Cundong Fan[a] and Tianfeng Chen*[a]

In the present study, two zinc(II) complexes containing bis-benzimidazole derivatives, $Zn(bpbp)Cl_2$ (**1**) and $[Zn(bpbp)_2](ClO_4)_2{\cdot}CH_3CH_2OH{\cdot}H_2O$ (**2**) (bpbp = 2,6-bis(1-phenyl-1*H*-benzo[*d*]imidazol-2-yl)pyridine), have been designed, synthesized and evaluated for their *in vitro* anticancer activities. The underlying molecular mechanisms through which they caused the cancer cell death were also elucidated. The complexes were identified as potent antiproliferative agents against a panel of five human cancer cell lines by comparing with cisplatin. Complex **2** demonstrated dose-dependent growth inhibition on MCF-7 human breast carcinoma cells with IC_{50} at 2.9 μM. Despite this potency, the complexes possessed great selectivity between human cancer cells and normal cells. Induction of apoptosis in MCF-7 cells by complex **2** was evidenced by accumulation of sub-G1 cell population, DNA fragmentation and nuclear condensation. Further investigation on intracellular mechanisms revealed that complex **2** was able to induce p53-dependent apoptosis in cancer cells by triggering DNA damage. On the basis of this evidence, we suggest that Zn(II) complexes containing bis-benzimidazole derivatives may be candidates for further evaluation as chemotherapeutic agents for human cancers.

Received 22nd December 2012,
Accepted 7th February 2013

DOI: 10.1039/c3dt33077j

www.rsc.org/dalton

Introduction

In the past decades, much attention has been paid to the interaction between small molecules and DNA.[1] DNA has been identified as a primary target for anticancer drug design and remains one of the most promising biological receptors for the development of chemotherapeutic agents. The interaction between small molecules and DNA could probably cause DNA damage in cancer cells, which in turn blocked cell division and finally results in cell death.[2] Therefore, the design of effective and selective DNA binding agents is essential for development of new potential DNA-targeted antitumor drugs. Till now, a large number of DNA-targeted drugs, such as 5-fluorouracil, cisplatin and a series of non-platinum metal complexes have been prepared. These kinds of agents exhibited their therapeutic effects on cancer cells by induction of DNA damage and activation of downstream signaling pathways.[3]

With the successful application as anticancer drugs, metal complexes, especially cisplatin, have stimulated extensive investigations and the search for alternative transition metal complexes with anticancer activities.[4] Recently, many metal-based compounds, such as Pt and Ru complexes, have been found to exhibit desirable antitumor activities.[5] However, the accumulation of metal ions in the body can lead to deleterious effects and unavoidable toxicity. Thus biodistribution and clearance of the metal complex as well as its pharmacological specificity need to be considered.[6]

As a vital metal ion for cellular processes, zinc (Zn), the second most important transition metal in the human body, is essential for cell growth and cell division.[7] Studies have showed that several families of regulatory proteins containing Zn were important for DNA synthesis, gene expression, and induction of cell apoptosis.[8] Recently, evidence also suggested an intriguing link between zinc and cancer.[9] For instance, increase in the Zn level could decrease the proliferation of

[a]*Department of Chemistry, Jinan University, Guangzhou, 510632, P. R. China. E-mail: tchentf@jnu.edu.cn, tzhwj@jnu.edu.cn*
[b]*Department of Chemistry Science and Technology, Zhanjiang Normal University, Zhanjiang, 524048, P. R. China*

†Electronic supplementary information (ESI) available: Experimental details for synthesis of ligand (bpbp) and crystallographic data for the complexes. CCDC 874326 (bpbp), 874327 (complex **1**), 874328 (complex **2**). For ESI and crystallographic data in CIF or other electronic format see DOI: 10.1039/c3dt33077j

‡Authors contributed equally to the work.

prostate cancer cells.[10] Zn has been shown to be responsible for the functional conformation of tumor suppressor p53, and the addition of physiological Zn concentrations could mediate the renaturation of wild-type p53.[11] However, little attention has been paid to the biological roles of synthetic Zn-based compounds, especially those containing bioactive molecules and exhibiting both effective antitumor and DNA-targeted activities.

Because DNA has been identified as a key pharmacological target of chemotherapeutic agents, many DNA-targeting groups such as intercalators have been conjugated to the metal ions in the past years.[6,12] The development of metal complexes containing bioactive molecules as ligands offers the possibility of discovering novel anticancer drugs with enhanced and targeted biological activities.[4a] Studies have showed that the intercalating abilities of the complexes depended on the types of metal ions, the ligand donor atoms, the planarity of ligands and the coordination geometry.[13] Benzimidazole derivatives are important pharmacophores in drugs that display a diversity of pharmacological activities, such as anti-inflammatory, antioxidant, gastroprotective and antiparasitic activities.[14] Many DNA minor groove binders containing one or more benzimidazole heterocycles, endowed with promising antitumor and antiparasitic activities, have been reported to date.[15] In our previous study, a series of Ru complexes containing bis-benzimidazole derivatives were synthesized and found to be able to target mitochondria and induce caspase-dependent apoptosis in cancer cells through superoxide overproduction.[16] Because both Zn and benzimidazole derivatives had potential in anticancer design, the combination of them in a single molecule could probably achieve enhanced anticancer effects. Interestingly, in the present study, two zinc(II) complexes containing bis-benzimidazole derivatives have been synthesized and evaluated for their *in vitro* anticancer activities. The underlying molecular mechanisms by which they caused cancer cell death were also elucidated. The results revealed that the complexes were able to induce p53-dependent apoptosis in cancer cells by triggering DNA damage in an intercalating mode. Therefore, the Zn(II) complexes containing bis-benzimidazole derivatives may be candidates for further evaluation as a chemotherapeutic agent for human cancers.

Results and discussion

Synthesis and molecular structural characterization of Zn complexes

The ligand bpbp (bpbp = 2,6-bis(1-phenyl-1*H*-benzo[*d*]imidazol-2-yl)pyridine) and two new Zn complexes were prepared following the method shown in Scheme S1.† The ligand bpbp was synthesized by displacement of the Br atom of bromobenzene by the deprotonated 2,6-bis(benzimidazole)pyridine. The reaction of bpbp with one equivalent of $ZnCl_2$ in DMF resulted in complex **1**. The reaction of two equivalents of bpbp with $Zn(ClO_4)_2$ in ethanol yielded complex **2**. The IR spectra for the free ligand bpbp, complex **1** and complex **2** showed all absorption bands resulting from the skeletal vibration of the aromatic rings in the 1392–1590 cm^{-1}. The appearance of 1439 and 1455 cm^{-1} of ligand and complexes are assigned to the vibration of C=N bond. The ligand and complexes gave satisfactory ^1H NMR spectra and element analysis. By comparing with bpbp, the δ values of H atom in complexes **1** and **2** shifted to the lower field.

The molecular structures of the ligand and complexes were established by X-ray crystallography as shown in Fig. 1. The crystal data are summarized in ESI Table S1.† Selected bond lengths and angles of complexes **1** and **2** are listed in Tables S2–S4,† respectively. As illustrated in Fig. 1A, two benzene rings of the ligand bpbp substituted the N–H bond of hydrogen atoms of benzimidazole groups. The average N–C bond length between substituted benzene rings and nitrogen atoms was 1.4364 Å. The substituted rings, benzimidazole rings and pyridine rings were not in the same plane. The dihedral angle between the substituted ring plane and the benzimidazole plane was 68.7°. As illustrated in Fig. 1B, the central Zn(II) ion was pentacoordinated and surrounded by N_3Cl_2 environment, adopting distorted trigonal bipyramidal geometry.

The ligand (bpbp) afforded three N atoms to coordinate to Zn(II) and two chloride ions located on each side of the planar pyridine ring. The bond angles of N(1)–Zn(1)–N(4), N(3)–Zn(1)–N(4) and N(3)–Zn(1)–N(1) were 144.52(10)°, 72.44(9)° and 72.10(9)°, respectively. The average bond length of Zn–N was 2.170(3) Å. The Zn(1)–Cl(1) and Zn(1)–Cl(2) bond lengths were 2.2558(10) Å and 2.2731(10) Å, respectively. The two benzimidazole rings and the pyridine ring in the ligand were nearly in the same plane (r.m.s. deviation = 0.3196 Å). The two substituted phenyl rings were inclined with the two benzimidazole rings. The dihedral angles between the substituted phenyl rings and the benzimidazole rings were 45.1° and 57.4°, respectively. The ORTEP drawing for complex **2** with atom numbering is shown in Fig. 1C, which demonstrates that complex **2** is a mononuclear structure and consists of a $[Zn(bpbp)_2]^{2+}$ dication, ClO_4^- counter anion, ethanol and water solvent molecule. In the $[Zn(bpbp)_2]^{2+}$ cation, the central Zn(II) ions adopted a distorted octahedral geometry with all six coordination positions occupied by six nitrogen atoms from two bpbp ligands. The longest and shortest bond lengths for Zn–N were 2.191 Å (Zn1–N9) and 2.117 Å (Zn1–N3) respectively, while the average bond length for Zn–N was recorded at 2.150 Å. The dihedral angle between the plane formed by Zn1 N1 N3 N4 and the plane formed by Zn1 N6 N8 N9 (r.m.s. deviation = 0.0197 Å) was 95.9°. The four substituted phenyl rings were inclined with the benzimidazole rings being attached. The dihedral angles between the substituted phenyl rings and the benzimidazole rings were 67.3°, 74°, 57.4° and 59.1°, respectively. Taken together, the clear characterization of the structure of the complexes facilitates the clarification of the antitumor mechanisms and the structure–activity relationship.

In vitro cytotoxic effects of Zn complexes

Studies have shown that metal complexes may act by enhancing the delivery of the active ligands to target sites inside the

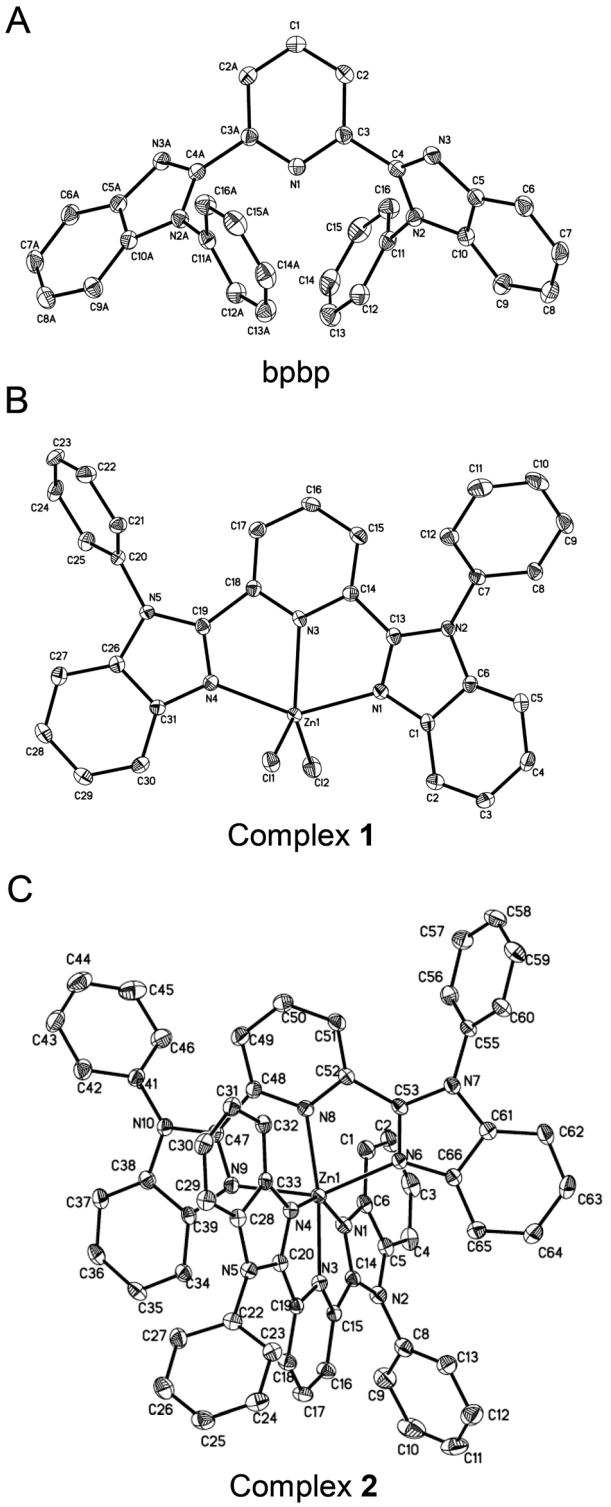

Fig. 1 Crystal structures of complexes studied in this work. (A) The molecule structure of bpbp (ORTEP; 30% ellipsoids; hydrogen atoms removed for clarity). (B) The molecule structure of complex **1** (ORTEP; 50% ellipsoids; hydrogen atoms removed for clarity). (C) Molecular structure of complex **2**. All unlabeled atoms are carbon atoms (ORTEP; 30% ellipsoids; hydrogen atoms removed for clarity).

cells.[17] Coordination of organic compounds with known therapeutic values to metal ions is an approach to the discovery of new metal-based drugs. The metal could probably act as a carrier and stabilizer for the drug ligands until it reaches its target. At the same time, the organic drug ligands could protect the metal and prevent side reactions in its transit toward a second target of biological action. Therefore, the combined effects between the metal and the ligands could result in enhancement of biological activities or activate new action mechanisms. For instance, the coordination of a well-known breast cancer drug tamoxifen to iron achieved significant enhancement of anticancer effects.[18] In the present study, benzimidazole derivatives were used as active ligands to be coordinated to Zn, because this kind of compound has been identified as an important pharmacophore in drug design and has been found to demonstrate promising anticancer activities and DNA-binding properties. The antiproliferative activities of the complexes were screened by MTT assay against a panel of five human cancer cell lines, including human breast adenocarcinoma MCF-7 cells, human osteosarcoma MG-63 cells, human cervix adenocarcinoma Hela cells, human melanoma A375 cells and human liver cancer Hep G2 cells. As the balance between therapeutic potential and toxic side effects of a compound is important for evaluating its usefulness as a pharmacological drug, experiments were also carried out to examine the cytotoxicity of the synthetic complexes against human normal cell lines. Therefore, HK-2 human kidney cells were chosen to evaluate the cytotoxicity for these compounds. As shown in Table 1, the ligand and the synthetic Zn complexes exhibited broad-spectrum inhibition on the growth of five human cancer cell lines with IC_{50} values ranging from 2.9 μM to 18.1 μM after a 72 h treatment, by using cisplatin as a positive control. The results demonstrated that the tested cancer cell lines were all susceptible to the ligand and complexes. Especially, complex **2**, containing two active ligands, was more active than complex **1** and the ligand itself toward all the tested cell lines. The IC_{50} value of MCF-7 cells was found at 2.9 μM, which was significantly lower than that of cisplatin and the ligand bpbp. These results suggest the contribution of the ligands to the anticancer activity of complexes and confirm the enhancement between the metal and the ligand in this kind of complex. However, the exact metabolism pathways and the active forms of the complexes inside the cellular remain elusive, which will be the focus of our future study.

Despite this potency, the synthetic complexes and the ligand were less toxic to HK-2 human normal cells, with IC_{50} values found at 28.4, 23.7 and 14.1 μM respectively, which were slightly higher than that of cisplatin (10.3 μM). These results demonstrated the lower toxicity of the complexes than cisplatin. Taken together, our results suggest that the Zn complexes possess better selectivity between cancer and normal cells than cisplatin and have potential application in cancer chemotherapy.

Induction of apoptotic cell death by complex 2

Because of the highest sensitivity of MCF-7 cells towards complex **2**, this cell line was used for further investigation on the underlying mechanisms of complex **2**-induced cell growth

Table 1 Growth inhibition of the ligand and complexes on selected human cancer and normal cells[a]

Compounds	IC_{50} (μM)					
	MCF-7	MG-63	HeLa	A375	Hep G2	HK-2[b]
bpbp	11.2 ± 1.3	15.9 ± 1.7	18.1 ± 2.9	14.6 ± 0.2	12.0 ± 0.9	28.4 ± 4.3
1	6.8 ± 1.5	5.2 ± 1.2	9.4 ± 0.5	9.5 ± 1.0	9.4 ± 0.2	23.7 ± 1.7
2	2.9 ± 0.3	3.6 ± 0.2	5.2 ± 0.5	5.4 ± 0.5	6.5 ± 0.2	14.1 ± 1.9
Cisplatin	3.0 ± 1.4	12.5 ± 2.1	15.9 ± 1.7	7.3 ± 0.8	13.6 ± 2.0	10.3 ± 2.1

[a] Cell viability after treatment for 72 h was determined by MTT assay as described in the Experimental section. Each IC_{50} value represents the mean ± SD of three independent experiments. [b] Human normal cells.

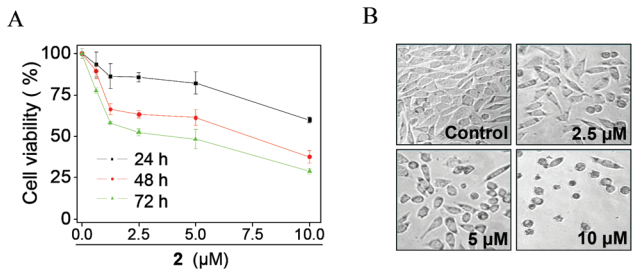

Fig. 2 Growth inhibition effects of complex **2** on MCF-7 cells. (A) Cells were treated with different concentrations of complex **2** for 24, 48, and 72 h and cell viability was examined by MTT assay. (B) Changes in the morphology of MCF-7 cells under different treatments of complex **2** for 72 h as examined by phase-contrast microscopy (magnification, 200×).

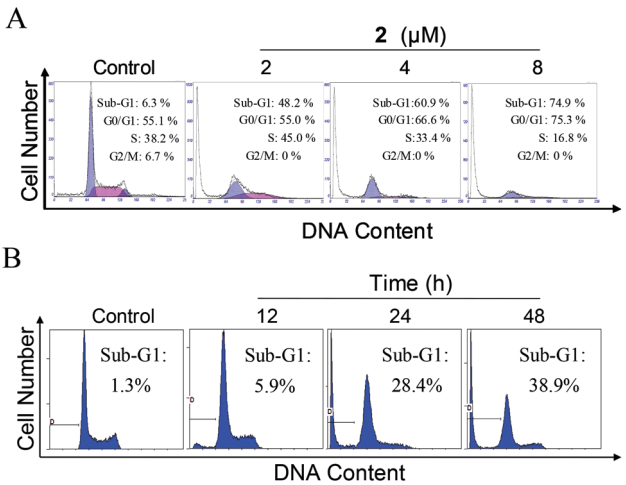

Fig. 3 Effects of complex **2** on cell apoptosis and cell cycle distribution in MCF-7 cells. (A) The cells treated with complex **2** for 72 h were collected and stained with PI after fixation. (B) Quantitative analysis of apoptotic cell death induced by complex **2** by measuring the sub-G1 cell population. Cells treated with 8 μM of complex **2** for various periods of time were fixed with 70% ethanol, stained with PI, and analyzed by flow cytometry. Each value represents the mean of three independent experiments.

inhibition. Generally the inhibition of cancer cell proliferation by anticancer drugs could be the result of induction of cell cycle arrest or apoptosis, or a combination of these two modes. Therefore in this study, firstly, the inhibitory effect of complex **2** on the growth of MCF-7 cells was also determined by MTT assay. As shown in Fig. 2A, treatment of MCF-7 cells with complex **2** resulted in a dose- and time-dependent inhibition of cell growth, accounting for 7–40, 11–62, and 22–71% inhibition after 24, 48, and 72 h of treatment with various concentrations of complex **2** (0.625–40 μM), respectively. In the phase-contrast observation, as shown in Fig. 2B, MCF-7 cells treated with different concentrations of complex **2** for 72 h showed dose-dependent decrement of cell numbers and the change in cell morphology, such as cell shrinkage, cell rounding, and the appearance of apoptotic bodies. Moreover, we determined the effect of complex **2** on cell cycle distribution using flow cytometry. As shown in Fig. 3A, exposure of MCF-7 cells to indicated concentrations of complex **2** resulted in marked dose-dependent increase in the proportion of apoptotic cells as reflected by the sub-diploid peaks. For instance, the sub-G1 population was noticeably enhanced from 6.3% to 74.9% after 72 h of treatment with 8 μM of complex **2**. Meanwhile, a slight increase in the G0/G1 phase population was also observed in cells exposed to 4 μM and 8 μM of complex **2**. The increase in the G0/G1 phase cell population was accompanied by a decrease in the S and G2/M phase cell populations. To study the time course for this increment of sub-G1 and G0/G1 phase cell populations, we treated the MCF-7 cells with 8 μM of complex **2** for various periods of time and analyzed by flow cytometry. As shown in Fig. 3B, complex **2** induced a noticeable time-dependent increase in the sub-G1 cell population, which reached 38.9% after the treatment for 48 h. However, no significant change in the cell cycle distribution was observed in the results (data not shown). On the whole, apoptosis could be a major mode of cell death induced by complex **2** in cancer cells. In order to further prove this finding, enzymatic labeling assay (TUNEL) and DAPI staining assay were carried out to detect DNA fragmentation and nuclear condensation. TUNEL can detect the early stage of DNA fragmentation in apoptotic cells prior to changes in morphology. Results shown in Fig. 4 reveal a dose-dependent increase in DNA fragmentation and nuclear condensation in MCF-7 cells. Taken together, these results demonstrate that the complex **2**-induced MCF-7 cell death is mainly caused by induction of apoptosis.

Induction of DNA damage in MCF-7 cells by complex 2

Accumulating evidence indicates that chemotherapeutic agents induced tumor regression through the inhibition of proliferation and/or the activation of apoptosis.[19] A broad array of metal complexes, especially cisplatin, with strong

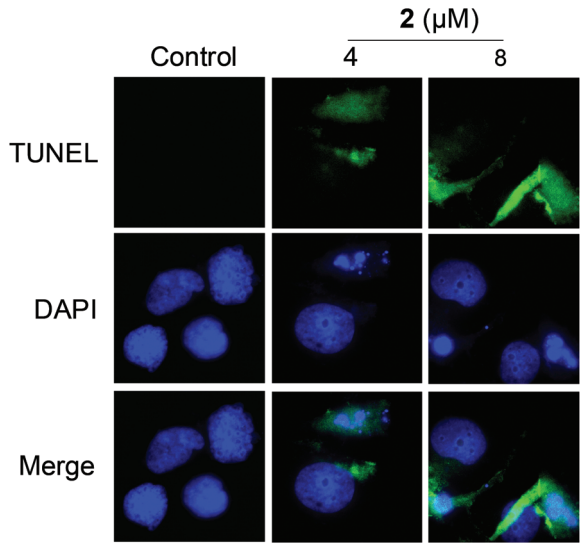

Fig. 4 Complex **2**-induced apoptotic cell death as examined by TUNEL and DAPI assay in MCF-7 cells. Cells were treated with different concentrations of complex **2** for 72 h. Representative images of DNA fragmentation and nuclear condensation in response to the treatment of complex **2** as described in Results and discussion (magnification, 200×).

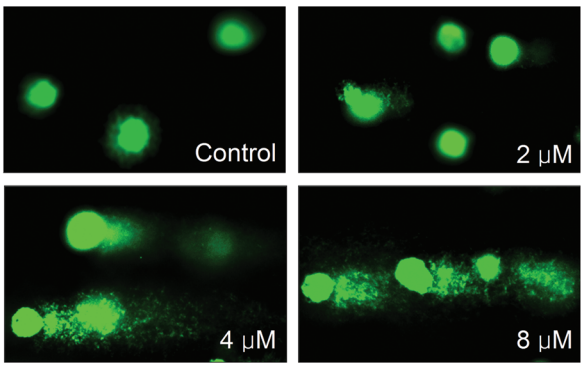

Fig. 5 Induction of DNA strand breaks in MCF-7 cells by complex **2**. Cells were treated with indicated concentrations of complex **2** for 12 h and then analyzed by Comet assay. The tail indicates cells with damaged DNA. The length of the tail reflects the degree of DNA damage. The images shown here are representative of three independent experiments with similar results.

DNA-binding behavior induce efficient apoptosis in cancer cells and many of them occurred with the involvement of DNA damage and direct interaction with DNA.[6,20] In our previous study,[16] Ru complexes containing bis-benzimidazole derivatives were found to be able to induce dose-dependent increase in DNA fragmentation and apoptosis in cancer cells. Based on these results, we predicted that complex **2**-induced MCF-7 cell apoptosis could be triggered by DNA damage. Therefore, the induction of DNA damage by complex **2** was investigated by Comet assay, which provides a simple and effective way to evaluate both single- and double-strand breaks in DNA at the single-cell level. Under the influence of an electric field, the denatured or cleaved DNA fragments can migrate out of the cells and display the amount of DNA present in the tail of the comet, which is representative of DNA damage caused by the added agent.[21] As shown in Fig. 5, a significant elevation of DNA strand breaks (DSBs) as evidenced by the increase in tail DNA was detected in MCF-7 cells. A dose-dependent increase in DNA damage was also observed in MCF-7 cells exposed to 2, 4 and 8 μM of complex **2** for 72 h. These results imply that DNA damage was triggered by complex **2** in cancer cells.

DNA-binding properties of complex 2

To further confirm the complex **2**-induced DNA damage in MCF-7 cells, the DNA-binding properties of complex **2** were also examined by spectroscopic and viscosity measurement. Spectrophotometry is the most common method to investigate the interaction of transition metal complexes with DNA. In general, transition metal complexes exhibit hypochromism and red shift in their electronic spectra when they are bound to DNA. The degree of hypochromism (decrease in absorption of the DNA band) depends on the binding mode and affinity.

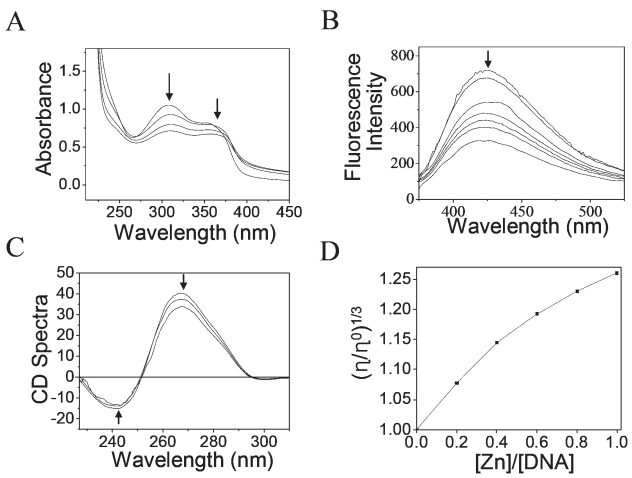

Fig. 6 DNA-binding behavior of complex **2** with DNA extracted from MCF-7 cells. (A) Absorption spectra of complex **2** in Tris-HCl buffer upon addition of increasing concentrations of MCF-7 cell DNA. [Zn] = 20 μM. (B) Emission spectra of complex **2** in 3 mM of Tris-HCl buffer in the absence and presence of MCF-7 cell DNA. [Zn] = 20 μM. (C) The CD spectra of MCF-7 cell DNA in absence or addition of increasing concentrations of complex **2**. [DNA] = 300 μM. (D) Effect of complex **2** on the relative viscosity of MCF-7 cell DNA at 30.0 °C (±0.1 °C). [DNA] = 400 μM.

With the addition of MCF-7 cell DNA, hypochromism (35%) and red shift ($\Delta\lambda$ = 3 nm) of MLCT transition (metal-to-ligand charge transition) of complex **2** in electronic spectra were observed (Fig. 6A). The calculated intrinsic binding constant (K_b) for complex **2** was 2.0×10^5 M^{-1}, which is typical for metal complexes that bind to DNA *via* intercalation. This result was further confirmed by fluorescence measurement in the absence or presence of different concentrations of MCF-7 cell DNA. The fluorescence intensity decreased obviously (Fig. 6B), which demonstrates the strong interaction between complex **2** and MCF-7 cell DNA. To gain further information, we also recorded the CD spectra of MCF-7 cell DNA exposed to complex **2** (Fig. 6C). The CD spectra showed a slight but significant decrease in the intensity of the positive CD signal

around 267 nm. The viscosity of the double strand DNA increases when a complex binds to DNA in an intercalating mode.[22] In order to further determine the binding mode, viscosity measurement was carried out by adding various concentrations of complex **2** to MCF-7 cell DNA. As shown in Fig. 6D, the relative viscosity of MCF-7 cell DNA increased significantly in the presence of complex **2**. Taken together, these results indicate that complex **2** may bind to DNA through an intercalating mode.

Complex 2 induces activation of the p53 pathway

Considerable evidence has shown that DNA damage could cause apoptotic cell death *via* various signaling pathways.[23] In cell models, DNA damage activates ATM (ataxia telangiectasia mutated) and ATR (ataxia telangiectasia and Rad3 related) proteins, which signal downstream to checkpoint kinases, such as CHK1 and CHK2, and tumor suppressor gene p53 and finally result in apoptosis.[24] As a transcription factor, p53, after activation by DNA damage,[25] could directly or indirectly induce cell apoptosis through both the extrinsic and intrinsic apoptosis pathways.[26] Based on the above evidences, it is possible that the DNA damage triggered by complex **2** may induce p53 phosphorylation. In order to confirm this hypothesis, we determined the protein level of total and phosphorylated p53 in MCF-7 cells after being treated with 2–8 μM of complex **2** for 72 h. As shown in Fig. 7, the treatments resulted in elevation of phosphorylated p53 at Ser15 in a dose-dependent manner. As another DNA damage maker, H2A.X was rapidly phosphorylated (within seconds) at serine 139 when DSBs are introduced into mammalian cells.[27] Therefore, we analyzed the phosphorylation of histone H2A.X on serine 139 by Western blotting. As shown in Fig. 7, a significant increase in this protein was observed in MCF-7 cells treated with indicated concentrations of complex **2**. These results suggest that the DNA damage-mediated p53 activation is involved in cancer cell apoptosis induced by complex **2**.

Due to the stability of these Zn(II) complexes being an important factor affecting their clinical applications in medicine, we detected the stability of the synthesized ligand (bpbp), complex **1** and complex **2** during the incubation in DMSO at room temperature (25 °C) for 72 h by UV-Vis. As shown in Fig. S1,† no change in the UV-Vis spectra of the ligand and complexes was observed. The ligand and complexes remained stable at least for 72 h. Based on these results, we confirmed that the solvolysis does not appear when dissolving the ligand and complexes in DMSO, which means it does not influence the results of biological studies. This stability supports their future applications in the treatment of cancers.

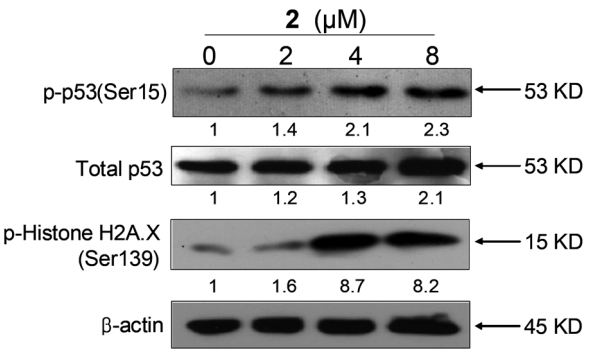

Fig. 7 Regulation of phosphorylated p53, total p53 and phosphorylated histone H2A.X expression levels by complex **2** in MCF-7 cells. Cells were exposed to complex **2** with indicated concentrations for 72 h. Changes in the levels of protein expression were shown as ratios of selected groups. All experiments were carried out at least in triplicates.

Conclusions

In the present study, two Zn(II) complexes containing bis-benzimidazole derivatives have been designed, synthesized and evaluated for their *in vitro* anticancer activities. The underlying molecular mechanisms through which they caused cancer cell death were also elucidated. The complexes were identified as potent antiproliferative agents against a panel of five human cancer cell lines. Especially, complex **2** demonstrated higher growth inhibition on MCF-7 human breast carcinoma cells than cisplatin. Despite this potency, the complexes possessed high selectivity between human cancer and normal cells, in comparison with cisplatin. Further investigation on intracellular mechanisms revealed that complex **2** was able to induce p53-dependent apoptosis in cancer cells by triggering DNA damage. On the basis of this evidence, we suggest that Zn(II) complexes containing bis-benzimidazole derivatives may be candidates for further evaluation as a chemotherapeutic agent for human cancers. This study provides broader space for improving the structure–activity relationships of Zn complexes and opens up a new dimension in the biomedical area for complexes in design of DNA-targeted anticancer agents.

Experimental section

Materials

Pyridine-2,6-dicarboxyl acid, *o*-phenylenediamine, bromobenzene, CuI, Cs_2CO_3, and 1,10-phenanthroline were purchased from Shanghai Aladin Reagent Company. All the chemicals and solvents were analytically pure and were used without further purification. Thiazolyl blue tetrazolium bromide (MTT), propidium iodide (PI), 4′,6-diamidino-2-phenylindole (DAPI) and a bicinchoninic acid (BCA) kit for protein determination were purchased from Sigma-Aldrich. All antibodies used in this study were purchased from Cell Signaling Technology (Beverly, MA). The water used in cellular experiments was ultrapure, supplied by a Milli-Q water purification system from Millipore.

Synthesis and characterizations

2,6-Bis(1-phenylbenzimidazol-2-yl)pyridine (bpbp). The ligand was synthesized according to a previous method.[31] Briefly, a mixture of bromobenzene (1.75 g, 11 mmol), 2,6-bis-

(benzimidazolyl)pyridine (1.65 g, 5.0 mmol), CuI (0.40 g, 2.1 mmol), 1,10-phenanthroline (0.8 g, 0.88 mmol), and Cs_2CO_3 (14.5 g, 45 mmol) was suspended in 50 ml of DMF. The mixture was refluxed for 24 h and then cooled to room temperature. The resulting sticky residue was purified by column chromatography (1 : 2 THF–hexane) and gave a colorless ligand (1.14 g, yield: 45%). The crystals were obtained from the evaporation of the ethanol solution. Selected IR data (KBr, cm^{-1}): 3422, 3058, 1597, 1503, 1439, 1392, 1336, 1250, 997, 752. ^1H NMR: ($CDCl_3$): 6.99 (d, 4H), 7.184–7.367 (m, 12H), 7.876 (t, 3H), 8.08 (d, 2H).

[Zn(bpbp)Cl$_2$] (1). A solution of $ZnCl_2$ (0.136 g, 1.0 mmol) in 10 ml of ethanol was added to a hot stirred solution of bpbp (0.464 g, 1.0 mmol) in 50 ml of ethanol. The reaction mixture was stirred for 20 minutes at room temperature. After recrystallization from ethanol, colourless crystals were obtained. Yield 0.240 g (80%). Anal. calcd for $C_{31}H_{21}Cl_2N_5Zn$ ([Zn(bpbp)Cl_2]): C, 62.07%; H, 3.53%; N, 11.68%. Found: C, 62.29%; H, 3.51%; N, 11.73%. Selected IR data (KBr, cm^{-1}): 3460, 3067, 1597, 1494, 1455, 1408, 1336, 1005, 750, 697. ^1H NMR: (d^6-DMSO): 7.21 (d, 4H), 7.49 (q, 12H), 8.01 (m, 3H), 8.06 (d, 2H).

[Zn(bpbp)$_2$](ClO$_4$)$_2$·CH$_3$CH$_2$OH·H$_2$O (2). A solution of Zn-$(ClO_4)_2{\cdot}6H_2O$ (0.186 g, 0.5 mmol) in 10 ml of ethanol was added to a hot solution of bpbp (0.464 g, 0.5 mmol) in a 50 ml ethanol solution. The reaction mixture was stirred for 20 minutes at room temperature. After recrystallization from ethanol, colourless crystals were obtained. Yield 0.505 g (80.67%). Anal. calcd for $C_{64}H_{50}Cl_2N_{10}O_{10}Zn$ ([Zn(bpbp)$_2$]-$(ClO_4)_2{\cdot}CH_3CH_2OH{\cdot}H_2O$): C, 72.76%; H, 4.77%; N, 13.26%. Found: C, 72.29%; H, 4.51%; N, 12.93%. Selected IR data (KBr, cm^{-1}): 3437, 3058, 1590, 1502, 1439, 1329, 1084, 744, 682, 618. ^1H NMR: (d^6-DMSO): 8.08 (t, 2H), 7.59 (m, 4H), 7.42 (d, 28H), 7.21 (d, 8H).

X-ray crystallography

Single crystal structure determination for the ligand and complexes **1** and **2** was performed on a Siemens Smart-CCD diffractometer equipped with a normal focus, 3 kW sealed tube X-ray source and graphite monochromated Mo-K_α radiation (λ = 0.71073 Å) at 173 K. The structures were solved by direct methods by using the program SHELXTL. Absorption correction was carried out by semi-empirical method, Fourier difference techniques, and refined by full-matrix least-squares. All non-hydrogen atoms in both structures were refined anisotropic displacement parameters. All hydrogen atoms were theoretically added.

Cell culture

The cell lines used in this study, including human breast adenocarcinoma MCF-7 cells, human osteosarcoma MG-63 cells, human cervix adenocarcinoma Hela cells, human melanoma A375 cells, human liver cancer Hep G2 cells and the normal human kidney HK-2 cells, were obtained from American Type Culture Collection (ATCC, Manassas, VA) and maintained in DMEM medium supplemented with fetal bovine serum (10%), penicillin (100 units ml^{-1}), and streptomycin (50 units ml^{-1}) at 37 °C in a humidified incubator with 5% CO_2 atmosphere.

MTT assay

The effects of the complexes on cell proliferation were determined by MTT assay. Briefly, cells were seeded in 96-well culture plates at different densities. After 24 h, different concentrations of compounds were added and incubated for the indicated time. Then, 20 μl per well of MTT solution (5 mg ml^{-1} phosphate buffered saline) was added and incubated for 5 h. The medium was aspirated and replaced with 200 μl per well of DMSO to dissolve the formazan salt formed. The color intensity of the formazan solution, which reflects the cell growth condition, was measured at 570 nm using a microplate spectrophotometer (VERSA max).

Flow cytometric analysis

Induction of apoptosis by complex **2** was quantified by flow cytometric analysis according to our previous method.[28] Briefly, treated or untreated cells were trypsinized, washed with PBS and fixed with 70% ethanol overnight at −20 °C. The fixed cells were washed with PBS and incubated with a PI working solution (1.21 mg ml^{-1} Tris, 700 U ml^{-1} RNase, 50.1 μg ml^{-1} PI, pH 8.0) for 4 h in darkness. The stained cells were analyzed with an Epics flow cytometer (Beckman Coulter, Fullerton, CA). Cell cycle distribution was analyzed using Multi-Cycle software (Phoenix Flow Systems, San Diego, CA). The proportion of cells in G0/G1, S, and G2/M phases was represented as DNA histograms. Apoptotic cells with a hypodiploid DNA content were measured by quantifying the sub-G1 peak in the cell cycle pattern. For each experiment, 10 000 events per sample were recorded.

TUNEL–DAPI co-staining assay

DNA fragmentation was examined by the TUNEL apoptosis detection kit (Roche) following the manufacturer's instruction. Briefly, cells cultured in chamber slides were fixed with 3.7% formaldehyde for 1 h and permeabilized with 0.1% Triton X-100 in PBS. Then, the cells were incubated with 50 μl of TUNEL reaction mixtures for 1 h at 37 °C. For nuclear staining, cells were incubated with 1 mg ml^{-1} of DAPI for 15 min at 37 °C. Stained cells were then washed with PBS and examined on a fluorescence microscope (Nikon Eclipse 80i).

Comet assay

Comet assay for detection of DNA damage was performed using a kit (Trevigen). According to our previous method,[29] cells treated with complex **2** were harvested by trypsinization, centrifuged and suspended in PBS. The cell suspensions mixed with melted LM agarose were coated on the standard slides and electrophoresis was performed for 30 min in a Savant ps 250 system set at 300 mA and 1 V cm^{-1} in darkness. After electrophoresis, the slide was rinsed with distilled water, fixed in 70% ethanol for 5 min and air-dried overnight. DNA was stained with SYBR Green I (Trevigen) and visualized under a fluorescence microscope (Nikon, Eclipse E-600).

DNA binding experiments

DNA binding experiments were done in Tris-HCl/NaCl buffer (5 mM Tris-HCl, 50 mM NaCl, pH 7.2) using DMSO solution of the complexes. The DNA was extracted from MCF-7 cells using a Mammalian genomic DNA extraction kit (Beyotime). Briefly, A375 cells were harvested by centrifugation at 2000 rpm. The cell pellets were suspended in lysis buffer containing protease and vortexed with the presence of phenol. Then the DNA was separated from other cell components. After addition of a 1 : 1 mixture of ethanol and ammonium acetate and shaking, DNA was precipitated and then washed with 75% ethanol twice. The obtained DNA was resuspended with nuclease-free water for further use. Solutions of DNA in Tris-HCl/NaCl buffer gave a ratio of UV absorbance (260/280 nm) of 1.8–1.9 : 1, indicating that the DNA was sufficiently free of protein. The concentration of DNA diluted 100-folds was determined spectrophotometrically by using the molar absorption coefficient of 6600 M^{-1} cm^{-1} (260 nm).

Absorption spectra of the synthetic complex **2** were recorded on a Cary 5000 UV-2450. Spectroscopic titrations were carried out by keeping a constant concentration of complex **2** (20 μM) dissolved in 3.0 ml of Tris-HCl buffer (pH 7.2, [NaCl] = 50 mM) with increasing concentrations of MCF-7 cell DNA. Each spectrum was recorded after equilibration of the sample for 10 min. The absorbance (A) of the most red-shifted band of complex **2** was recorded after successive additions of MCF-7 cell DNA. The intrinsic equilibrium binding constant (K_b) values were calculated according to the decay of the Soret absorption by eqn (1).[30]

$$(\varepsilon_a - \varepsilon_f)/(\varepsilon_b - \varepsilon_f) = (b - (b^2 - 2K_b{}^2C_t[\mathrm{DNA}]/s)^{1/2})/2K_bC_t \quad (1)$$

where $b = 1 + K_bC_t + K_b[\mathrm{DNA}]/2s$ and ε_a is the extinction coefficient observed for the spectral band at a given DNA concentration, ε_f is the extinction coefficient of the complex free in solution, ε_b is the extinction coefficient of the complex when fully bound to DNA, K_b is the equilibrium binding constant, C_t is the total complex concentration, [DNA] is the DNA concentration in nucleotides and s is the fitting parameter giving an estimate of the binding site size in base pairs. The non-linear least-squares analysis was done using OriginLab.

Emission spectra of the synthetic complex **2** were measured on a 970CRT spectrofluorometer with excitation at 363 nm. Spectroscopic titrations were carried out under room temperature to determine the binding affinity between DNA and complex **2**. Briefly, 3.0 ml of Tris-HCl buffer (pH 7.2, [NaCl] = 50 mM) was placed in the reference cuvette and complex **2** (20 μM), dissolved in 3.0 ml of Tris-HCl buffer (pH 7.2, [NaCl] = 50 mM), was added into the sample cuvette. Then the MCF-7 cell DNA at 2.0 mM in base pairs was added into both the reference and the sample cuvettes. Finally, the spectra were recorded in the range of 373–700 nm.

The circular dichroism (CD) spectra of MCF-7 cell DNA modified by complex **2** were recorded on a Jasco J-810 spectrophotometer equipped with a thermoelectrically controlled cell holder. The cell path length was 1 cm. Spectra were recorded in the range of 230–500 nm in 0.2 nm increments with an averaging time of 1 s. CD spectral characteristics were compared for MCF-7 cell DNA in the absence and presence of complex **2**, respectively.

Viscosity measurements were carried out using a Schott Gerate AVS 310 automated viscometer maintained at 30.0 ± 0.1 °C in a thermostatic bath. The increasing concentrations of complex 2 were added into 400 μM of DNA solution. The flow time was measured by a digital timer and each sample was measured three times. The relative viscosity of DNA in the absence and presence of the metal complex was calculated using eqn (2).

$$\eta = (t - t_0)/t_0 \quad (2)$$

where t is the flow time of the DNA-containing solution with different concentrations of complex **2** and t_0 is the flow time of the DNA-containing solution alone. Data are presented as $(\eta/\eta^0)^{1/3}$, where η^0 is the viscosity of DNA in the absence of complex **2** and η is the viscosity of DNA in the presence of complex **2**.

Western blot analysis

The cells were harvested after centrifugation, washed with PBS twice. Total cellular proteins were extracted by incubation of cell pellets with cell lysis buffer (Cell Signaling Technology) overnight at −20 °C. The protein concentrations of the extracts were determined using a BCA protein assay kit according to the manufacturer's instructions. SDS-PAGE was done in 12% tricine gels loading 40 μg of cell lysates per lane. After electrophoresis, separated proteins were transferred to nitrocellulose membranes for 75 min at 110 V and blocked with 5% non-fat milk in TBS buffer for 1 h. Then, the membranes were washed with TBST buffer and incubated with primary antibodies at 1 : 1000 dilutions in 5% BSA overnight at 4 °C with continuous agitation; secondary antibodies were conjugated with horseradish peroxidase at 1 : 5000 dilutions for 2 h at room temperature, followed by three washes in TBST buffer. The target proteins were detected on X-ray film (Kodak) using an enhanced chemiluminescence reagent. β-Actin was used to confirm the equal loading and transfer of proteins.

Statistical analysis

Experiments were carried out at least in triplicate and results were expressed as mean ± SD. Statistical analysis was performed using the SPSS statistical program version 13 (SPSS Inc., Chicago, IL). The difference between two groups was analyzed by a two-tailed Student's t test. A difference with $P < 0.05$ (*) or $P < 0.01$ (**) was considered statistically significant.

Acknowledgements

This work was supported by the Natural Science Foundation of China and Guangdong Province, the Program for New Century Excellent Talents in University, Key Project of Science and

Technology Department of Guangdong Province, the Fundamental Research Funds for the Central Universities and Grant of State Key Laboratory of Oncology in South China.

Notes and references

1 (*a*) C. Tan, J. Liu, H. Li, W. Zheng, S. Shi, L. Chen and L. Ji, *J. Inorg. Biochem.*, 2008, **102**, 347–358; (*b*) Y. M. Song, Q. Wu, P. J. Yang, N. N. Luan, L. F. Wang and Y. M. Liu, *J. Inorg. Biochem.*, 2006, **100**, 1685–1691.
2 S. M. Hecht, *J. Nat. Prod.*, 2000, **63**, 158–168.
3 R. Palchaudhuri and P. J. Hergenrother, *Curr. Opin. Biotechnol.*, 2007, **18**, 497–503.
4 (*a*) P. C. Bruijnincx and P. J. Sadler, *Curr. Opin. Chem. Biol.*, 2008, **12**, 197–206; (*b*) L. Kelland, *Nat. Rev. Cancer*, 2007, **7**, 573–584; (*c*) M. Markman, *Expert. Opin. Drug Saf.*, 2003, **2**, 597–607.
5 (*a*) T. Chen, Y. Liu, W. J. Zheng, J. Liu and Y. S. Wong, *Inorg. Chem.*, 2010, **49**, 6366–6368; (*b*) F. S. Mackay, J. A. Woods, H. Moseley, J. Ferguson, A. Dawson, S. Parsons and P. J. Sadler, *Chem.–Eur. J.*, 2006, **12**, 3155–3161; (*c*) I. Berger, M. Hanif, A. A. Nazarov, C. G. Hartinger, R. O. John, M. L. Kuznetsov, M. Groessl, F. Schmitt, O. Zava, F. Biba, V. B. Arion, M. Galanski, M. A. Jakupec, L. Juillerat-Jeanneret, P. J. Dyson and B. K. Keppler, *Chem.–Eur. J.*, 2008, **14**, 9046–9057; (*d*) W. X. Ni, W. L. Man, S. M. Yiu, M. Ho, M. T. W. Cheung, C. C. Ko, C. M. Che, Y. W. Lam and T. C. Lau, *Chem. Sci.*, 2012, **3**, 1582–1588.
6 C. X. Zhang and S. J. Lippard, *Curr. Opin. Chem. Biol.*, 2003, **7**, 481–489.
7 B. L. Vallee and K. H. Falchuk, *Physiol. Rev.*, 1993, **73**, 79–118.
8 (*a*) J. E. Coleman, *Curr. Opin. Chem. Biol.*, 1998, **2**, 222–234; (*b*) T. V. O'Halloran, *Science*, 1993, **261**, 715–725.
9 (*a*) V. Sharma, D. Anderson and A. Dhawan, *Apoptosis*, 2012, **17**, 852–870; (*b*) G. D'Orazi and D. Givol, *Cell Cycle*, 2012, **11**, 2581–2582.
10 P. Feng, T. L. Li, Z. X. Guan, R. B. Franklin and L. C. Costello, *Prostate*, 2002, **52**, 311–318.
11 (*a*) Y. Cho, S. Gorina, P. D. Jeffrey and N. P. Pavletich, *Science*, 1994, **265**, 346–355; (*b*) C. Meplan, M. J. Richard and P. Hainaut, *Oncogene*, 2000, **19**, 5227–5236; (*c*) O. Margalit, A. J. Simon, E. Yakubov, R. Puca, A. Yosepovich, C. Avivi, J. Jacob-Hirsch, I. Gelernter, A. Harmelin, I. Barshack, G. Rechavi, G. D'Orazi, D. Givol and N. Amariglio, *Int. J. Cancer*, 2012, **131**, 562–568; (*d*) X. Yu, A. Vazquez, A. Levine and D. Carpizo, *Cancer Cell*, 2012, **21**, 614–625.
12 (*a*) H. K. Liu and P. J. Sadler, *Acc. Chem. Res.*, 2011, **44**, 349–359; (*b*) L. Li, W. Cao, W. Zheng, C. Fan and T. Chen, *Dalton Trans.*, 2012, **41**, 12766–12772.
13 A. M. Pyle and J. K. Barton, *Prog. Inorg. Chem.*, 1990, **38**, 413–475.
14 M. Boiani and M. Gonzalez, *Mini-Rev. Med. Chem.*, 2005, **5**, 409–424.
15 (*a*) A. Joubert, X. W. Sun, E. Johansson, C. Bailly, J. Mann and S. Neidle, *Biochemistry*, 2003, **42**, 5984–5992; (*b*) J. Mann, A. Baron, Y. Opoku-Boahen, E. Johansson, G. Parkinson, L. R. Kelland and S. Neidle, *J. Med. Chem.*, 2001, **44**, 138–144.
16 L. Li, Y. S. Wong, T. Chen, C. Fan and W. Zheng, *Dalton Trans.*, 2012, **41**, 1138–1141.
17 (*a*) C. S. K. Rajapakse, A. Martinez, B. Naoulou, A. A. Jarzecki, L. Suarez, C. Deregnaucourt, V. Sinou, J. Schrevel, E. Musi, G. Ambrosini, G. K. Schwartz and R. A. Sanchez-Delgado, *Inorg. Chem.*, 2009, **48**, 1122–1131; (*b*) R. A. Sanchez-Delgado and A. Anzellotti, *Mini-Rev. Med. Chem.*, 2004, **4**, 23–30.
18 (*a*) A. Nguyen, S. Top, P. Pigeon, A. Vessieres, E. A. Hillard, M.-A. Plamont, M. Huche, C. Rigamonti and G. Jaouen, *Chem.–Eur. J.*, 2009, **15**, 684–696; (*b*) A. Nguyen, A. Vessieres, E. A. Hillard, S. Top, P. Pigeon and G. Jaouen, *Chimia*, 2007, **61**, 716–724.
19 T. S. Kim, B. Y. Yun and I. Y. Kim, *Biochem. Pharmacol.*, 2003, **66**, 2301–2311.
20 (*a*) K. R. Barnes and S. J. Lippard, *Met. Ions Biol. Syst.*, 2004, **42**, 143–177; (*b*) L. Zhang, Y. Zhang, P. Y. Huang, F. Xu, P. J. Peng and Z. Z. Guan, *Cancer Chemother. Pharmacol.*, 2008, **61**, 33–38; (*c*) H. Robson, S. Meyer, S. M. Shalet, E. Anderson, S. Roberts and O. B. Eden, *Med. Pediatr. Oncol.*, 2002, **39**, 573–580.
21 D. W. Fairbairn, P. L. Olive and K. L. O'Neill, *Mutat. Res.*, 1995, **339**, 37–59.
22 (*a*) S. Satyanarayana, J. C. Dabrowiak and J. B. Chaires, *Biochemistry*, 1992, **31**, 9319–9324; (*b*) S. Satyanarayana, J. C. Dabrowiak and J. B. Chaires, *Biochemistry*, 1993, **32**, 2573–2584.
23 W. P. Roos and B. Kaina, *Trends Mol. Med.*, 2006, **12**, 440–450.
24 A. Sancar, L. A. Lindsey-Boltz, K. Unsal-Kacmaz and S. Linn, *Annu. Rev. Biochem.*, 2004, **73**, 39–85.
25 M. Yamaguchi, N. Fujimori-Tonou, Y. Yoshimura, T. Kishi, H. Okamoto and I. Masai, *Development*, 2008, **135**, 1247–1257.
26 L. J. Hofseth, S. P. Hussain and C. C. Harris, *Trends Pharmacol. Sci.*, 2004, **25**, 177–181.
27 E. P. Rogakou, D. R. Pilch, A. H. Orr, V. S. Ivanova and W. M. Bonner, *J. Biol. Chem.*, 1998, **273**, 5858–5868.
28 T. Chen, W. Zheng, Y. S. Wong and F. Yang, *Biomed. Pharmacother.*, 2008, **62**, 77–84.
29 T. Chen and Y. S. Wong, *Cell. Mol. Life Sci.*, 2008, **65**, 2763–2775.
30 (*a*) A. M. Angeles-Boza, P. M. Bradley, P. K. Fu, S. E. Wicke, J. Bacsa, K. R. Dunbar and C. Turro, *Inorg. Chem.*, 2004, **43**, 8510–8519; (*b*) J. D. McGhee and P. H. von Hippel, *J. Mol. Biol.*, 1974, **86**, 469–489.
31 H. Wang, P. He, S. Liu, J. Shi and M. Gong, *Inorg. Chem. Commun.*, 2010, **13**, 145–148.

